April 2021

Investigating Structural Proteins by Light Scattering

Uma Nudurupati

Investigating Structural Proteins by Light Scattering

Uma Nudurupati

INVESTIGATING STRUCTURAL PROTEINS BY LIGHT SCATTERING

A Thesis Presented

by

Uma Nudurupati

Submitted to the Graduate School of the
University of Massachusetts Amherst in partial fulfillment of the requirements for the degree of

MASTER OF SCIENCE

February 2021

Department of Chemistry

INVESTIGATING STRUCTURAL PROTEINS BY LIGHT SCATTERING

A Thesis Presented

by

Uma Nudurupati

Approved as to style and content by:

_____

Murugappan Muthukumar, Chair

_____

Michael D. Barnes, Member

_____

Ricardo Metz , Head of the Department

Department of Chemistry

DEDICATION

To the Brahman

ACKNOWLEDGMENTS

My graduate experience at UMass Amherst has been an incredible experience of learning and self-discovery. It was not a solo effort. It wouldn't have been possible for me to move across the globe to pursue an education but for my parents' unconditional support. Amma and Appa, you are the wind beneath my wings. Friendships that I forged in Amherst have been pivotal to my survival in outside the lab, and I am genuinely grateful to all of them. Thank you, Kartik, Sandhya, Subhalakshmi, Sohini, Rik, and Nikita.

Academically, I learned about problem formulation and solution approaches immensely at the Polymer Science and Engineering department. Specifically, I would like to thank Professor Muthukumar for being my advisor and for his support through this journey. I would also like to thank Professor David Hoagland for the many conversations on scattering literature, my data, and instrumentation. I would also like to extend my thanks to my labmates in the Muthu lab, especially Zach, Kate, and Di.

None of this would have been possible without the support of my parent department, Department of Chemistry. Professor DV, and Professor Michael Barnes, thank you for your constructive feedback.

ABSTRACT

INVESTIGATING STRUCTURAL PROTEINS BY LIGHT SCATTERING

FEBRUARY 2021

Uma Nudurupati, B.S.-M.S., UNIVERSITY OF HYDERABAD, INDIA

M.S., UNIVERSITY OF MASSACHUSETTS AMHERST

Directed by: Professor Murugappan Muthukumar

This thesis evaluates the organization of the structural proteins, Human Gamma D crystallin and Collagen type II, into higher-order structures using light scattering. Specifically, it evaluates the natures of incipient aggregation in Human Gamma D crystallin and the nature of its interactions with CAPEGn, an electrostatic blocker. Additionally, this thesis evaluates whether Collagen type II growth kinetics follows Classical nucleation theory.

TABLE OF CONTENTS

Page

ACKNOWLEDGMENTS vii

ABSTRACT viii

LIST OF TABLES xi

LIST OF FIGURES xii

Introduction 2

Experimental background 3

Dynamic Light Scattering for Ergodic systems 3

Affinity Chromatography 6

Chapter 1: Human Gamma D aggregation and its prevention by additives 7

Introduction 7

CA$(PEG)_n$: Electrostatic blockers 8

Materials and Methods 9

Results and Discussion 10

Human Gamma D Crystallin (dilute solution) Characteristics 10

Effect of C.A. (PEG)n on Human Gamma D Crystallin 12

Effect of the size of the PEG spacer 12

Effect of concentration of C.A. $(PEG)_4$ 13

Other Modifiers 14

Sodium Lipoate 14

Pantetheine 15

N-Acetyl Cysteine amide 16

16

Menadione sodium bisulfite 17
Conclusions 19
Chapter 2: Collagen type II fibrogenesis 20
Method 23
Instrumentation 23
Sample preparation 24
Timing the experiment 26
Data Analysis 27
Results and discussion 29
Concentration dependence of growth kinetics 30
Temperature dependence of growth kinetics 32
Conclusions 34
Appendix 1: Factors influencing light scattering in Poly Acryl amide acrylate gels 36
Introduction 36
Methods 36
Synthesis of Poly (acrylamide-co-sodium acrylate) gel 36
Swelling the gel for light scattering 38
Method of Light scattering 39
Results and discussion 39
i. Variation in β as a function of crosslinking density of the crosslinker 39
ii. Variation in β as a function of charge density 40
41
iii. Variation in β as function of salt concentration of the swelling solution 41
Conclusions 42
References 43

LIST OF TABLES

Table Page

Table 1 Hydrodynamic radius of the various modes present in solutions containing different modifiers along with HGD 19

Table 2 Above table contains the specific amounts of the chemicals used to prepare a 10CX0.2 (10% charge density and 0.2 % crosslinking density) sample in a 10 mL volume vial 38

LIST OF FIGURES

Figure Page

Figure 1 Schematic diagram of the various possible fates of Human Gamma D crystallin protein....2

Figure 2 An example of intensity correlation function obtained during a DLS experiment....4

Figure 3 Field correlation function for a representative data set....5

Figure 4 (a) Correlation function for a solution of HGD (0.66 mg/ml) (b)Distribution function of HGD (0.66 mg/ml) at angles 30, 60 and 90. (c) Γ vs q2 for a dilute solution of HGD (0.66 mg/ml) 10

Figure 5 (a)Hydrodynamic radii of various modes as a function of Protein concentration (b)Distribution function of HGD at various concentrations at 35o (c) Γ vs q2 for dilute solutions of HGD at various concentrations....11

Figure 6 (a)Hydrodynamic radius of the mode observed, concentration of HGD, concentration of CA(PEG)n for various n (n= 1,2,3,4) (b)Distribution function of HGD with CA(PEG)n (n= 1,2,3,4) at 30o (c) Γ vs q2 for dilute solutions of HGD with CA(PEG)n (n= 1,2,3,4) 12

Figure 7 (a)Hydrodynamic radius of the modes observed vs various concentration of C.A. (PEG)4 (b) Γ vs q2 for the two modes in the dilute solution of HGD with C.A. (PEG)4 at various concentrations....13

Figure 8 (a) Γ vs q2 of the various modes observed in DLS (b) The distribution function of the various modes in DLS as observed on performing CONTIN fitting....14

Figure 9 (a) Γ vs q2 of the various modes observed in DLs for a solution of HGD and Pantethiene (b) Γ vs q2 of the various modes observed in DLS for HGD solution alone....15

Figure 10(a) The distribution function of the solution of HGD containing Pantethine as observed in CONTIN at various angles. (b) The distribution function of the solution of HGD (control) as observed in CONTIN at various angles....15

Figure 11 The distribution function of Sodium lipoate from CONTIN fitting....16

Figure 12(a) Γ vs q2 of the various modes observed in DLs for a solution of HGD and N-Acetyl Cystine amide (b) Γ vs q2 of the various modes observed in DLS for HGD solution alone 16

Figure 13(a) The distribution function of the solution of HGD containing N-acetyl cysteine amide as observed in CONTIN at various angles. (b)) The distribution function of the solution of HGD (control) as observed in CONTIN at various angles 17

Figure 14 (a) Γ vs q2 of the various modes observed in DLs for a solution of HGD and Menadione sodium bisulfite (b) Γ vs q2 of the various modes observed in DLS for HGD solution alone 18

Figure 15 (a) The distribution function of the solution of HGD containing Menadione sodium bisulfite as observed in CONTIN at various angles. (b) The distribution function of the solution of HGD (control) as observed in CONTIN at various angles 18

Figure 16 Representative data for Collagen type II fibrogenesis measurement using Turbidity, where the lag phase of the kinetics is highlighted in gray and the growth phase in yellow. 21

Figure 17 Absorption spectrum of the matrix gels (10% Charge density 0.4% crosslinking density – 10CX0.4, 10% Charge density 0.6% crosslinking density – 10CX0.6, 10% Charge density 0.8% crosslinking density – 10CX0.8, and buffer solution 1xPBS) into which the Collagen type II fibers are to be grown 23

Figure 18 Turbidity measurement of Collagen type II 1.32 mg/mL in TrisHCl pH = 7.2 from a stock collagen solution stored for 3 days. 24

Figure 19 Turbidity measurement of Collagen type II (1.32 mg/mL) fiber growth in TrisHCl pH = 7.2 at 37 oC after no incubation (black) and 15 min equilibration at 20ºC displaying a peak at early time point 25

Figure 20 Collagen fibers formed on dialysis into Tris HCl solution 26

Figure 21 A graphic explaining the protocol of the experiment 27

Figure 22 A. Normalized turbidity as a function of time for Collagen 0.66 mg/mL in Tris HCl at 40°C, B. Lag time estimation by visual inspection C. Lag time estimation by calculation of first and second derivate by Forward Difference method. 28

Figure 23 Data for collagen concentration 0.165 mg/mL at 40 °C in black, the logistic fit in red, and the tangent drawn in the linear segment to estimate a 29

Figure 24 Collagen type II nucleation time decreases as a function of concentration at 40 ° C 30

Figure 25 Collagen type II growth rate displaying non-monotonic dependency on concentration at 40 ° C 30

Figure 26 Inverse of lag time and lnC plot for collagen fibrogenesis at 40 ° C 31

Figure 27 Collagen type II nucleation time decreases as a function of temperature at 0.165 mg/mL 32

Figure 28 Inverse ln(lag time) vs Temperature for Collagen concentration 0.165 mg/mL 33

Figure 29 Collagen type II growth rate as a function of temperature at 0.165 mg/mL 33

Figure 30 Inverse ln(Growth rate) vs Temperature for Collagen concentration 0.165 mg/mL 34

Figure 31. correlation function at θ = 30 degrees across 3 arbitrary orientations for 40

Figure 32 a. Correlation function at θ = 30 degrees across 3 arbitrary orientations for a. 10CX0.2 swollen in 1xPBS b. 20CX0.2 swollen in 1xPBS c. 10CX2.7 swollen in 1xPBS d. 20CX2.7 swollen in 1xPBS 41

Figure 33 a. Correlation function at θ = 30 degrees across 3 arbitrary orientations for 10CX2.7 gel swollen in a. 0.1 M NaCl b. 0.5 M NaCl and c. 1 M NaCl 41

INTRODUCTION

Proteins are naturally occurring hetero polymers that constitute of the primary work force in a cell. The roles that these macromolecules are dictated by their chiral monomers, amino acids, and their unique sequence. It is this sequence that directs its conformation or its fold. When in its correctly folded form it is in its 'native state' and possesses its unique abilities, that are attributed to its function.[1]

When the native state of the protein is disrupted either due to external or internal forces the protein unfolds. On unfolding its propensity to aggregate increases as its hidden hydrophobic residues are exposed. In the absence of chaperones that help re-fold unfolded proteins, these unfolded proteins aggregate together and under certain specific conditions to form fibrils. This aggregation of proteins has been an area of interest for generations of scientific research as it is associated with human health and diseases. (Figure 1)

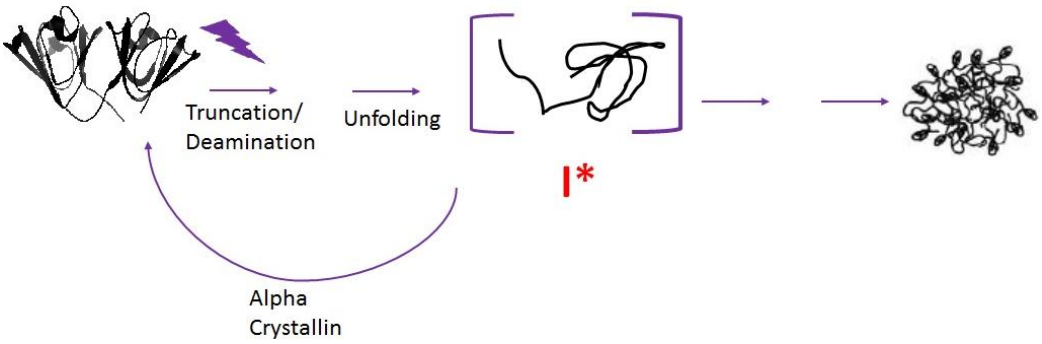

Figure 1 Schematic diagram of the various possible fates of Human Gamma D crystallin protein

The plethora of disease protein aggregation has been associated with ranges from Alzheimer's to cataracts. In this thesis, we investigate the organization of two structural proteins, Human Gamma D crystallin and Collagen type II, in dilute solutions at physiological conditions using light scattering. The aggregation of Human Gamma D has been associated

with cataracts[2], and a molecular understanding of the forces that cause this phenomenon would be critical to developing solutions to it. In our studies in Chapter 1, we have investigated the variation in the size of the Human Gamma D crystallin aggregates in the presence of additive that screen charges (CAPEG).

On the other hand, Collagen type II is known to organize into long fibers that provide support by maintaining tissue integrity and load distribution[3]. Specifically, it is present in the vitreous humor, and the degeneration of the vitreous humor has been related to structural changes in the collagen fiber. An understanding of the Collagen fiber growth phenomenon would enhance the fundamental understanding of the biosynthesis of the vitreous humor. In Chapter 2, we evaluate whether the Collagen type II fibrogenesis follows nucleation-growth kinetics by measuring turbidity as a function of time.

The next section is a short discussion on the primary method of investigation, dynamic light scattering, and affinity chromatography.

Experimental background

Dynamic Light Scattering for Ergodic systems

Dynamic Light Scattering (DLS) provides information about the particles performing Brownian motion, both translational and rotational. This technique is typically used to estimate the diffusion coefficient for a particle and hence obtain an estimate for its hydrodynamic radius. The hydrodynamic radius estimated by this technique lies in the range of an nm to more than a few micrometers.

In the experiment, real-time fluctuations in light intensity are measured as a function of time ($g_2(q,\tau)$), resulting in data similar to figure 2. These fluctuations are attributed to the change in solute concentration at the local scale because of their Brownian motion. Under

the infinite dilution limit, we assume that polymer solutions are governed by Brownian dynamics, as each polymer is far apart from the other.[4]

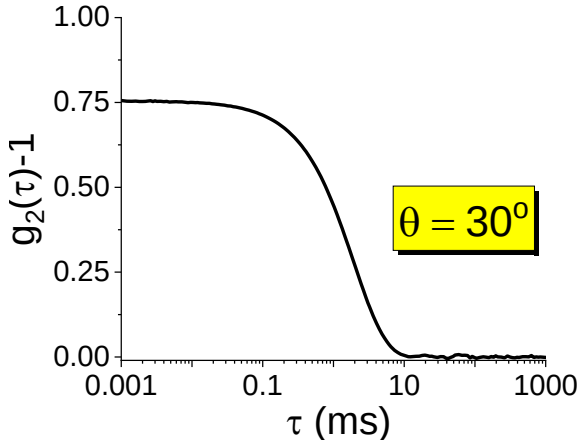

Figure 2 An example of intensity correlation function obtained during a DLS experiment.

Since the equations relate to the diffusion coefficient (D) of the system are all in terms of the electric field correlation function ($g_1(q,\tau)$)[5]. A relationship between the field correlation function and the intensity correlation function would enable us to calculate the diffusion coefficient from an experimentally measurable quantity ($g_2(q,\tau)$). For an ergodic system, these two are related using Siegert relation:

$$g_2(q,\tau) = B\,(1 + \beta|g_1(q,\tau)|^2) \quad \text{Eq. 1}$$

Here, the additional parameters are the baseline (B) and a factor β, which depends on the aperture radius of the detector and beam radius of the incident Laser. The light scattering setup is calibrated such that β is 1.

The software along with the ALV-5000 correlator calculates the $g_1(q,\tau)$ taking these factors into account, and then with the help of the CONTIN fitting algorithm, the field correlation is fitted to a sum of exponentials by the user.

$$g_1(q,\tau) = A * \exp(-\Gamma_1 t) + B * \exp(-\Gamma_2 t) \ldots \text{Eq. 2}$$

Here Γ_1 is the relaxation rate of a species present in the solution. Typically, in a system with two particles of sizes separately by order of magnitude will have a $g_1(q,\tau)$ that is a sum of two exponentials or is a bimodal distribution. For a system with monodisperse particle distribution, the field correlation function can be expressed as a single exponent, as seen in figure 3.

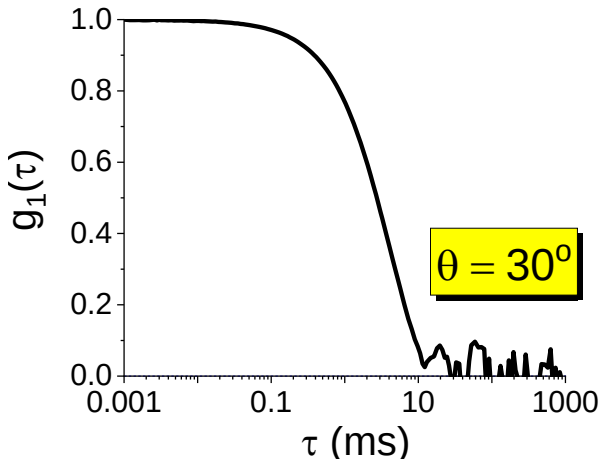

Figure 3 Field correlation function for a representative data set

The relaxation rates obtained by fitting the field correlation function are related to the diffusion coefficient, D by eq. 3, where q is the scattering vector.

The scattering vector is a function of the angle of scattering (θ), the wavelength of scattering (λ), and the refractive index of the solvent (n), as seen in equation 4.

$$\Gamma = Dq^2 \qquad \text{Eq. 3}$$

$$q = \frac{4\pi n \sin(\frac{\theta}{2})}{\lambda} \quad \text{Eq. 4}$$

Applying the Stokes Einstein Equation (eq. 5) in turn, provides the hydrodynamic radius for the diffusive particle of interest.

$$D = \frac{k_B T}{6\pi\eta R_h} \qquad \text{Eq. 5}$$

Affinity Chromatography

Affinity chromatography is used to purify proteins that bind specifically to a stationary phase. In this study, we utilize Nickle affinity chromatography. In this method, the stationary phase comprises of immobilized Ni ions, and a faction of lysed bacterial cells are passed over it to separate the protein of interest. The protein of interest bears a Histidine tag at one of the ends, C or N terminal, which is freely accessible which binds to the Ni on the column. The Ni stationary phase chelates with the Histidine tag, where the Histidine act as a ligand for the Ni^{2+}. Once the protein of interest is successfully bound to the column, the column is washed with higher concentrations of free imidazole to elute it. To prevent non-specific interaction of proteins in the cell lysate fraction with the column, the initial buffer in which the lysate is suspended in, binding buffer contains 20 mM of imidazole and 350 mM of NaCl.

CHAPTER 1: HUMAN GAMMA D AGGREGATION AND ITS PREVENTION BY ADDITIVES

Introduction

Aggregation of Human Gamma D crystalline (HGD) protein has been attributed to cataracts. In our studies, we focus on understanding the forces that control aggregation to develop molecules to suppress cataracts.

Many models describe the causes of aggregation of HGD. These models are classified into two categories, one where modifications or mutations on HGD result in aggregation-prone proteins and the other that affects the concentration of heat shock protein, alpha crystallin[6], a chaperon that is known to be associated with refolding of the protein.

In the former case, many mutations and post-translational modifications have been identified that are directly involved in specific physiological instances[7][8]. Moreover, many more have been developed to use as models to mimic the effects of external factors. For example, King Lab's W103E mutant mimics the U.V.- irradiation-induced cataracts, where it is known that the tryptophan residues are oxidized [9]. In the latter case, where there is a reduction in alpha-crystallin concentration with age, as the number of chaperons reduces, the unfolded HGD aggregates increase, and cataracts occur. To tackle cataracts from this front, peptides have been developed that are crucial fragments from the intact alpha-crystallin protein that is crucial to the chaperoning process. These peptides have been shown to have activity like that of the intact protein and have been suggested as a possible solution[10][11].

Our approach is universal, independent of the model of cataracts. In our previous studies, it has been shown that at dilute solution conditions, HGD forms an aggregate that is sensitive to the salt concentration in the solution and unfazed by the reducing

environment[12]. Using this insight, our lab hypothesized that electrostatics plays a crucial role in the incipient aggregation of HGD. Furthermore, to prevent aggregation, we have previously identified a charge masking agent $CA(PEG)_n$ [13]. In this chapter, investigations using the said masking agent with varying concentrations and linker size are reported. Additionally, the performance of $CA(PEG)_n$ is compared to other molecules expected to inhibit aggregation, as expected from the literature.

$CA(PEG)_n$: Electrostatic blockers

To understand the role of electrostatics in a protein's interaction with itself, we choose to study dilute solution characteristics of Human Gamma D crystallin (HGD). HGD's phase transitions and the cold cataract phenomena have been studied in detail by the Benedek Lab. One of their strategies to inhibit cataract formation was to chemically modify lens proteins with reagents that resulted in a significant reduction in phase transition temperature, a measure of inter-protein interactions.[14][15] Clark in the 1980s reported the reversible prevention of cold cataract, by a decrease in phase transition temperature, by polyols like glycerol and ethylene glycol, and irreversible prevention by glutaraldehyde, acetaldehyde, formaldehyde, and acrylamide[16]. Pande *et al*. have also shown that by modifying the -S.H. group bearing amino acids, cysteine, and methionine, with N-bromoacetylethanol aminephosphate, a highly polar and hydrophilic molecule, there was a drastic decrease in phase transition temperature[15]. When the same group tested an uncharged but polar molecule, N-ethymaleimide, they saw a decrease of phase transition only by 100 ^{o}C [17]. The drugs that have made it to the clinical trials are glutathione and its prodrugs that target the S.H. group, but these have not shown any significant result. The work from the Clark, Benedek and Pande point in the direction of hydrophilic molecules with charges but have little or no indication of the residues which they target. A wide variety of *in vivo* and *in vitro* experiments have been performed to test the effectiveness of micronutrients against

aggregation forming cataracts. However, the clinical trials undertaken to this day have shown negligible activity of these micronutrients against cataracts.[18]

Our strategy to prevent the aggregation of HGD is by using charged hydrophilic zwitterionic molecules Carboxyl Amine PEG, CAPEG, and its n-PEG chain analogs. This strategy is based on the hypothesis that CAPEGs are masking the charged residues on the surface of Human protein γ D crystallins[19][12]. This protein is decorated with acidic (glutamic acid aspartic acid) and basic (Lysine and arginine) residues on the surface, which at physiological pH bears charges. While the exact contribution of the forces that lead to the aggregation is still a question of debate, the PEG modifiers being studied require no carrier vehicle and biocompatible as well. This makes them an excellent choice for investigation. In the past, it has been shown by our lab that at dilute conditions (concentrations lower than those present in the human eye) on increasing the salt concentration, the aggregate disappeared, which lead to the above hypothesis.[12] Additionally, Benjamin Mohr has shown that at these concentrations, the addition of up to 5 mM of reductant DTT did not affect the aggregate's presence.

Materials and Methods

HGD protein was recombinantly expressed in m15 prep4 cells and purified using Ni-affinity column. The protein present in elution buffer was buffer exchanged into PBS buffer (20 mM Phosphates 150 mM NaCl pH = 6.8) using a HiTrap Desalting column. The protein solution so obtained was measured for concentration by measuring absorbance at 280 nm. This solution was then passed through a PVDF 0.2 um Low protein binding filter before placing in a flacon tube. To the tube of filtered protein solution, 100 mg of solid modifier powder was added, and the tube was placed at 4 ^{o} C overnight on a rocker. The next day, this

solution was filtered using a PVDF 0.2 um Low protein binding filter into a DLS tube, and the DLS experiment was performed.

Results and Discussion

Human Gamma D Crystallin (dilute solution) Characteristics

A dilute solution of Human Gamma D Crystallin (HGD) at physiological conditions (150 mM NaCl pH = 6.8) was found to contain two particle sizes as probed by Dynamic light scattering, as seen from the double peaks in the distribution function in figure 4(b).

One species is a fast mode typically of 2 nm hydrodynamic radius attributed to the isolated protein, and the other species, the slow mode, of around 55 nm is attributed to the aggregate. For example, DLS studies of a 0.66 mg/ml solution of HGD as in figure 4 (a). Both modes observed are diffusive, as seen in figure 4 (c).

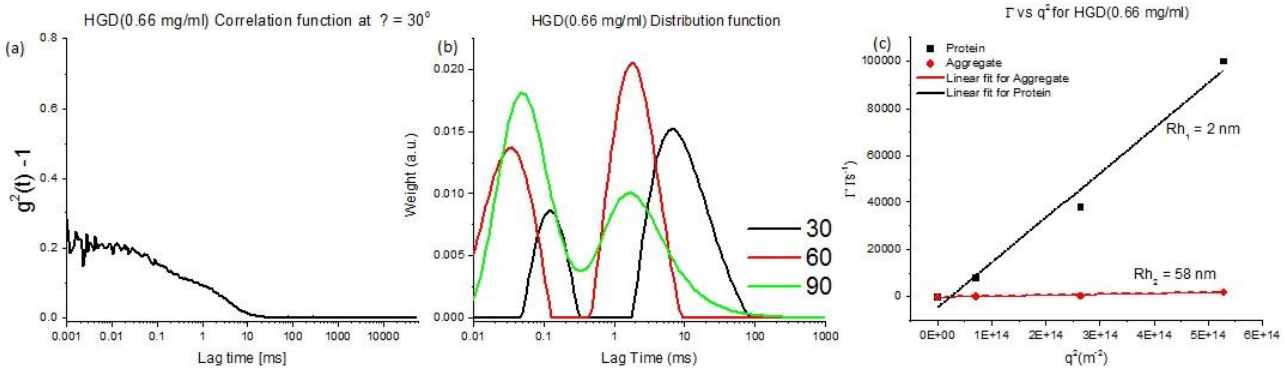

Figure 4 (a) Correlation function for a solution of HGD (0.66 mg/ml) (b)Distribution function of HGD (0.66 mg/ml) at angles 30, 60 and 90. (c) Γ vs q2 for a dilute solution of HGD (0.66 mg/ml)

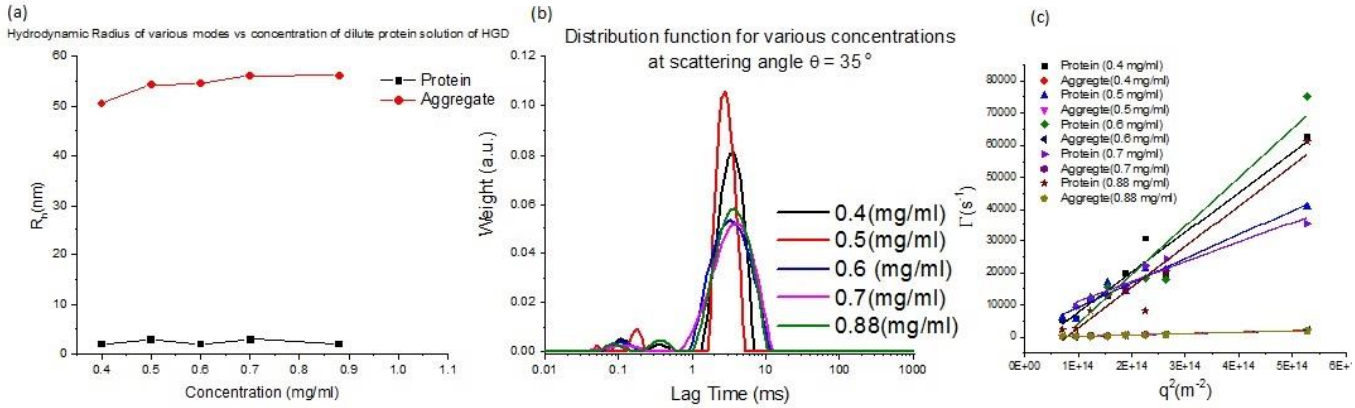

Figure 5 (a)Hydrodynamic radii of various modes as a function of Protein concentration (b)Distribution function of HGD at various concentrations at 35o (c) Γ vs q2 for dilute solutions of HGD at various concentrations

The two modes observed of HGD were observed irrespective of concentration from 0.4 mg/ml to 0.88 mg/ml, as can be seen in figure 4. The while the average size of the fast mode was 2 nm, the average size of the slow mode was 55 nm. This implied that the size of the aggregate in this concentration region was independent of HGD concentration, as seen in figure 5.

Effect of C.A. (PEG)n on Human Gamma D Crystallin

Effect of the size of the PEG spacer

On addition of C.A. $(PEG)_n$, the slow mode, as observed in the dilute solution of HGD was absent.

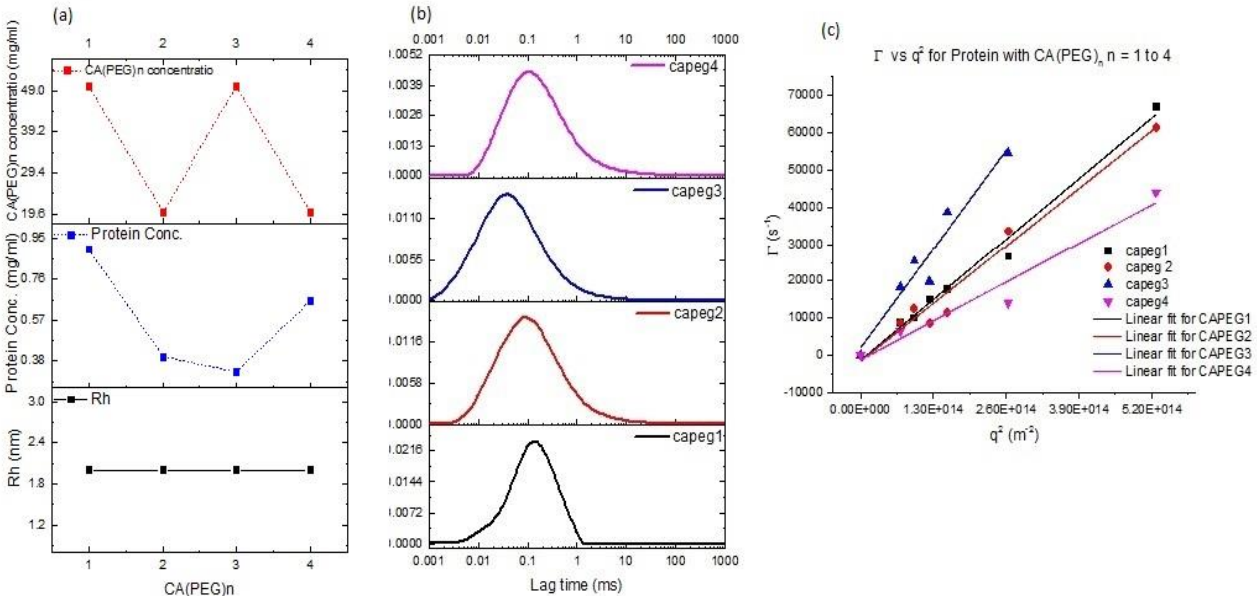

Figure 6 (a)Hydrodynamic radius of the mode observed, concentration of HGD, concentration of CA(PEG)n for various n (n= 1,2,3,4) (b)Distribution function of HGD with CA(PEG)n (n= 1,2,3,4) at 30o (c) Γ vs q2 for dilute solutions of HGD with CA(PEG)n (n= 1,2,3,4)

This absence of the slow mode was observed to be independent of the chain size of the PEG (n = 1,2,3, and 4) between the termini, as can be seen from the distribution functions in figure 6(b). The average size of the mode observed is ~ 2 nm, which are diffusive, as seen in figure 6 (c).

The concentration of C.A. $(PEG)_{n\ used}$ in the experiments was either 50 mg/ml (for n = 1, and 3) or 20 mg/ml (for n =2, and 4).

Effect of concentration of C.A. $(PEG)_4$

The effect of concentration of C.A. $(PEG)_4$ at a fixed concentration of HGD (0.9 mg/ml) was investigated. The concentrations that were probed, were 4 mg/ml, 8 mg/ml, 12 mg/ml, and 16 mg/ml; all below the previously used concentration of 20 mg/ml. At these lowered concentrations of C.A. $(PEG)_4$ a slow mode was persistently found, as can be seen from the distribution functions in fig. 7 (b) alongside with the presence the fast mode, the protein.

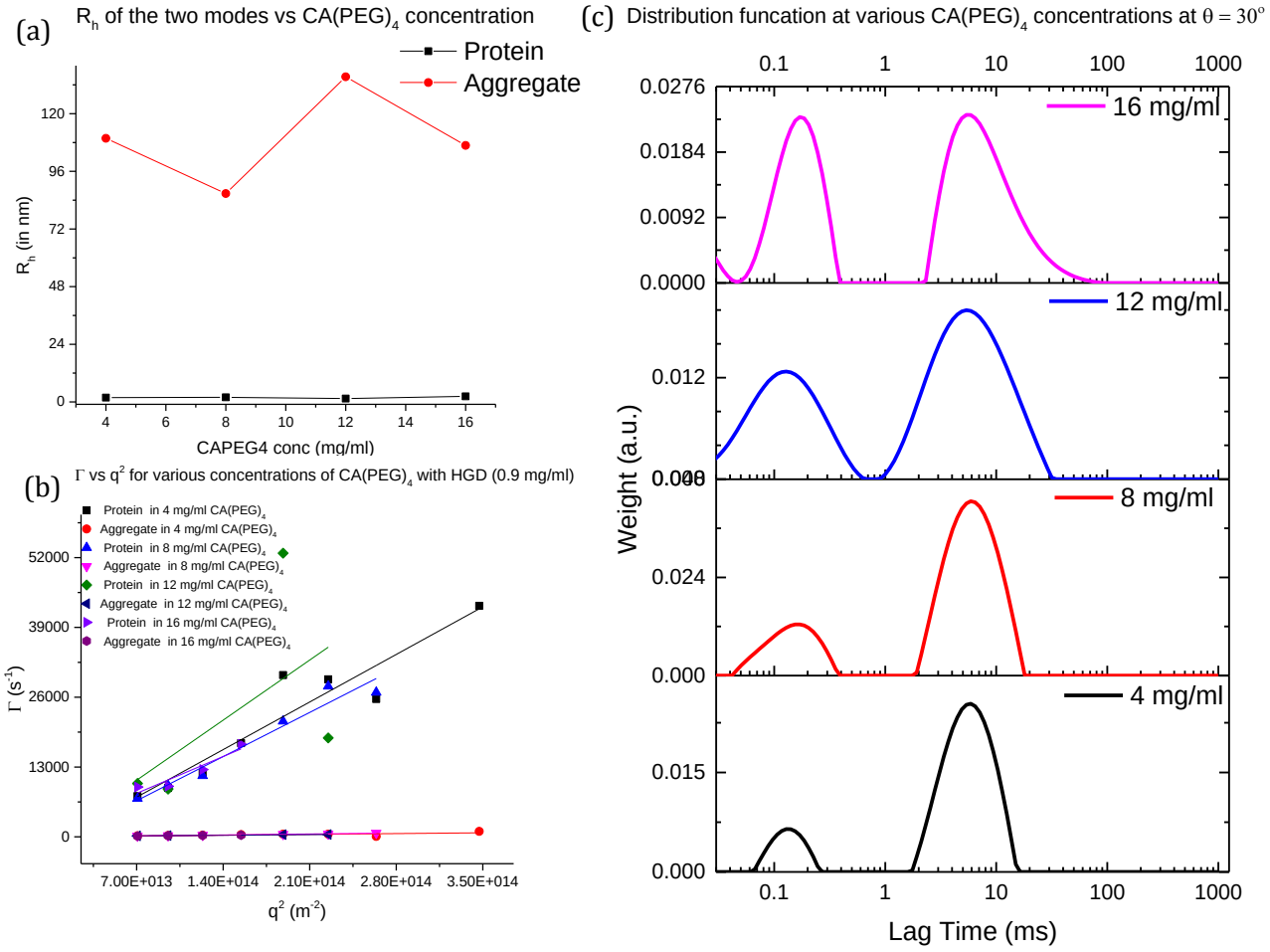

Figure 7 (a)Hydrodynamic radius of the modes observed vs various concentration of C.A. (PEG)4 (b) Γ vs q2 for the two modes in the dilute solution of HGD with C.A. (PEG)4 at various concentrations

Other Modifiers

Sodium Lipoate

In the presence on Sodium Lipoate the solution of HGD was shown to contain two modes of size 3 nm (red line in Figure 8(a)) and 10 nm (pink line in Figure 8 (a)) when fitted using HDRC.

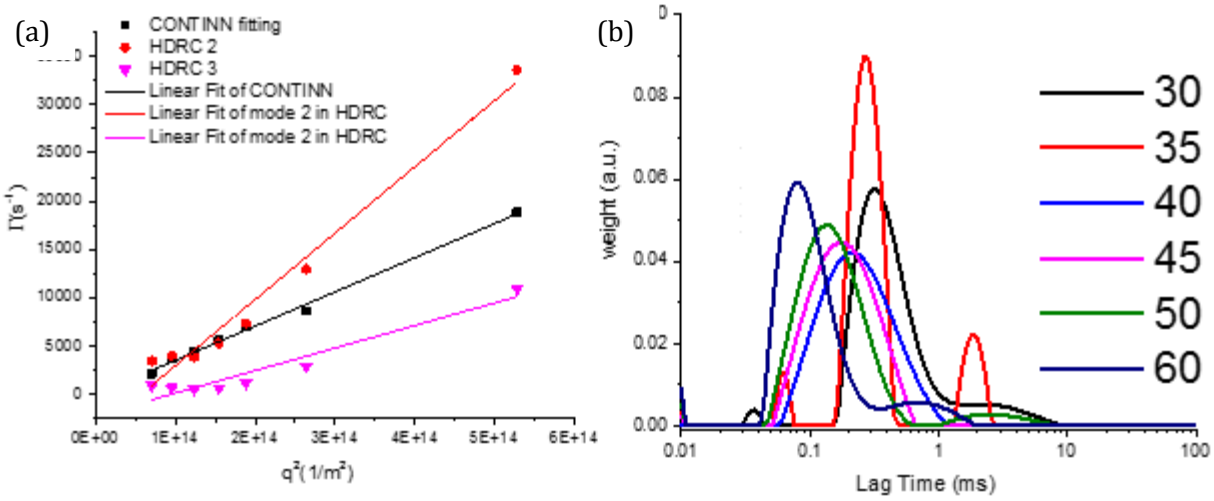

Figure 8 (a) Γ vs q2 of the various modes observed in DLS (b) The distribution function of the various modes in DLS as observed on performing CONTIN fitting

On fitting the data with CONTINN, only a single mode of 6 nm is observed. All the modes observed by DLS are diffusive as seen from the Γ vs q^2 plot in fig. 9(a). The second mode of 10 nm observed can be correlated to an arrangement that Sodium Lipoate forms by itself in the buffer. Based on this evidence, one can conclude, there are no aggregates of HGD in the presence of sodium Lipoate.

Pantetheine

In the presence on Pantetheine, the solution of HGD was shown to contain two modes of size 2 nm (red line in Figure 9(a)) and 47 nm (black line in Figure 9 (a)).

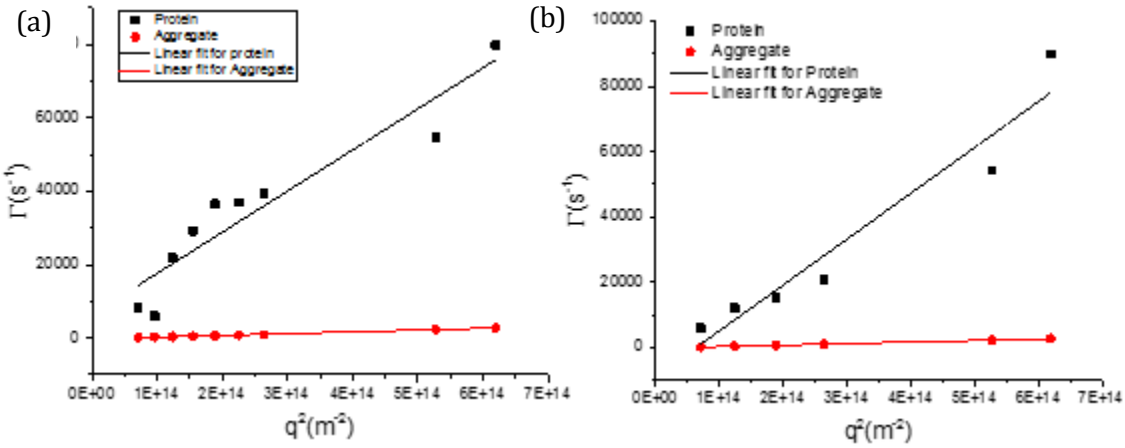

Figure 9 (a) Γ vs q2 of the various modes observed in DLs for a solution of HGD and Pantethiene (b) Γ vs q2 of the various modes observed in DLS for HGD solution alone

The aggregate in the presence of Pantetheine is of nearly the same size as of the aggregate (50 nm) found in control that contained no modifiers subjected to the same set

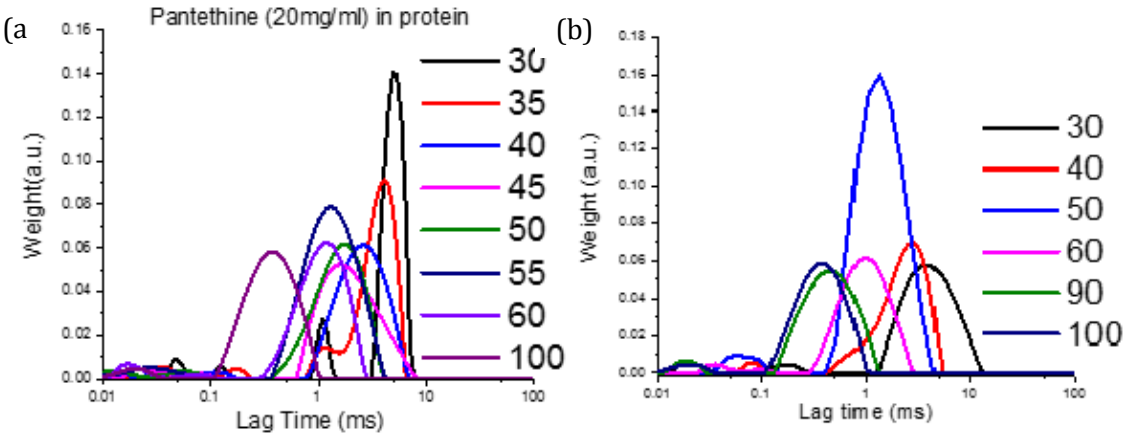

Figure 10(a) The distribution function of the solution of HGD containing Pantethine as observed in CONTIN at various angles. (b) The distribution function of the solution of HGD (control) as observed in CONTIN at various angles

of conditions. Both samples, the one with modifier and without the modifier, contained two diffusive modes as can be seen from Figure 10.

The distribution functions obtained from CONTIN fitting for the control and the Pantetheine containing solutions are very similar as well, as can be seen from Figure 11.

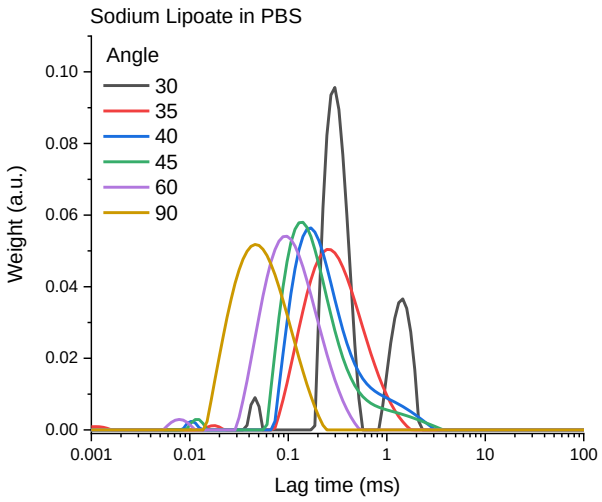

Figure 11 The distribution function of Sodium lipoate from CONTIN fitting

N-Acetyl Cysteine amide

In the presence on N-Acetyl Cysteine amide, the solution of HGD was shown to contain two modes of size 2 nm (red line in Figure 12 (a)) and 25 nm (black line in Figure 12 (a)).

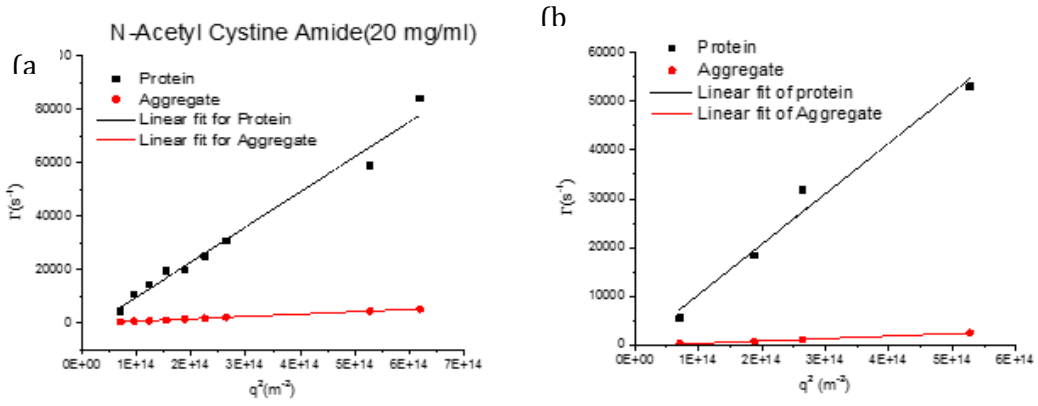

Figure 12(a) Γ vs q2 of the various modes observed in DLs for a solution of HGD and N-Acetyl Cystine amide (b) Γ vs q2 of the various modes observed in DLS for HGD solution alone

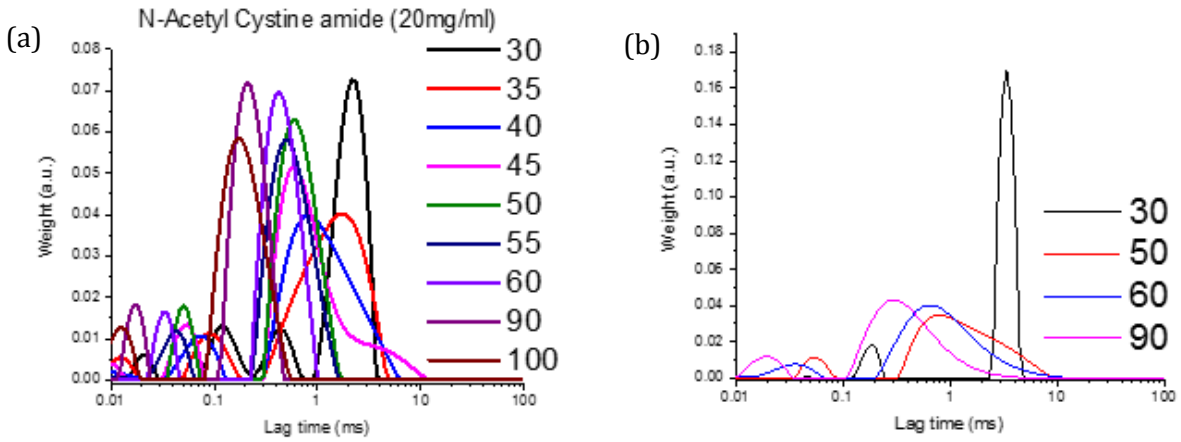

Figure 13(a) The distribution function of the solution of HGD containing N-acetyl cysteine amide as observed in CONTIN at various angles. (b)) The distribution function of the solution of HGD (control) as observed in CONTIN at various angles

The presence of an aggregate can be further confirmed from the presence of a slow mode after the addition of N-acetyl cysteine amide in the distribution function (figure 13) .

Menadione sodium bisulfite

In the presence on Menadione sodium bisulfite, the solution of HGD contained two modes of one of size 2 nm (red line in Figure 14 (a)) and another of 38 nm (black line in Figure 14 (a)). The aggregate in the presence of this modifier is of nearly half the size as of the aggregate (44 nm) found in control that contained no modifiers. Both samples, the one with modifier and without a modifier, contained two diffusive modes as seen in Figure 14.

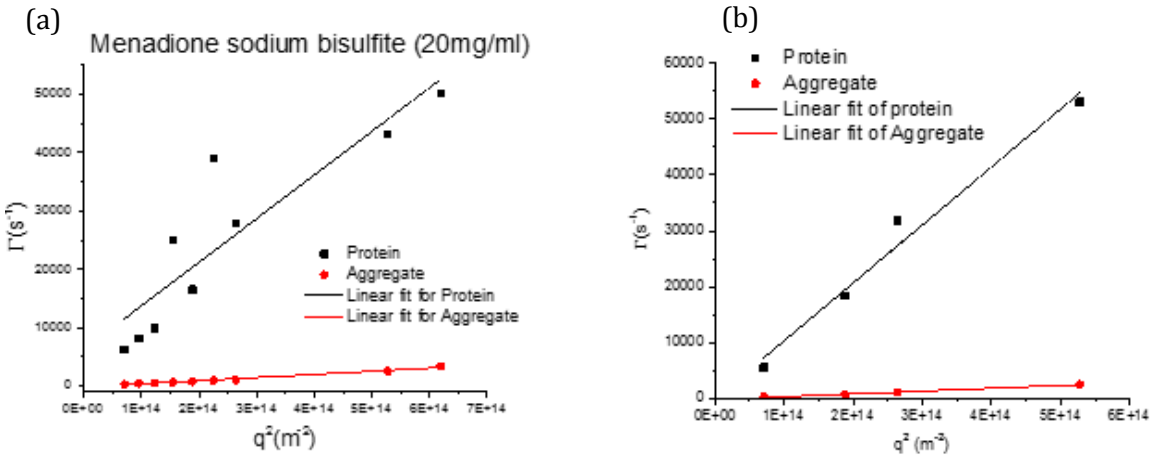

Figure 14 (a) Γ vs q2 of the various modes observed in DLs for a solution of HGD and Menadione sodium bisulfite (b) Γ vs q2 of the various modes observed in DLS for HGD solution alone

The distribution functions obtained from CONTIN fitting for the control and the Menadione sodium bisulfite containing solutions can be seen from Figure 15.

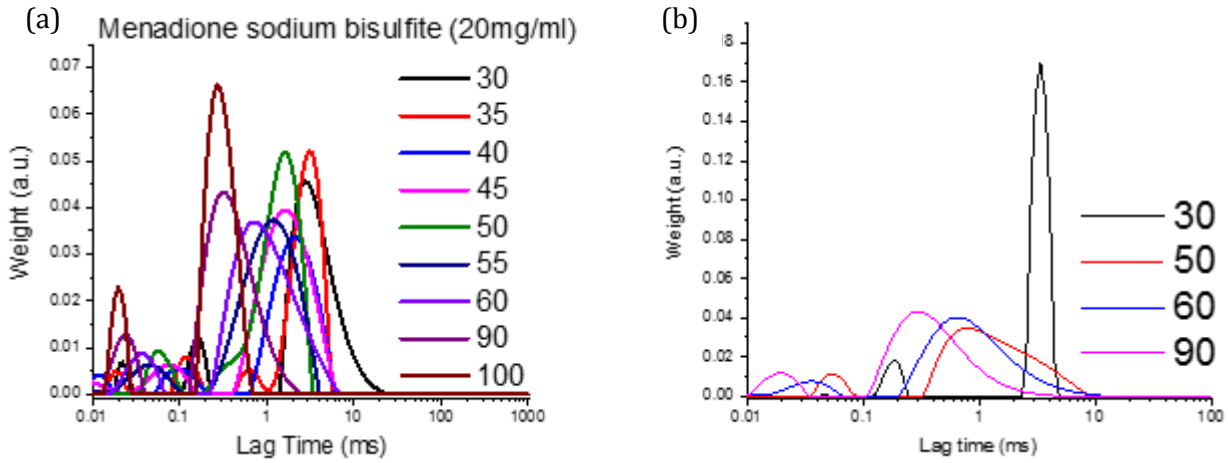

Figure 15 (a) The distribution function of the solution of HGD containing Menadione sodium bisulfite as observed in CONTIN at various angles. (b) The distribution function of the

Conclusions

Dilute solution of HGD contained two modes, a fast mode, attributed to the protein, and a slow mode attributed to an aggregate. This aggregate's size was found to be invariant to the concentration of HGD (within 0.4 mg/ml to 0.88 mg/ml range). On addition of C.A. $(PEG)_n$ (n = 1 to 4), the slow mode was absent. A summary of the various modes obtained for different additives can be seen in Table 1.

Additive added to protein	D1 (m^2/s)	Rh1 (In nm)	D2 (m^2/s)	Rh2 (in nm)	Method of fitting
$CA(PEG)_1$	1.25E-10	2	-	-	CONTIN
$CA(PEG)_2$	1.21E-10	2	-	-	CONTIN
$CA(PEG)_3$	2.04E-10	2	-	-	CONTIN
$CA(PEG)_4$	8.05E-11	~ 2	-	-	CONTIN
Pantetheine	1.12E-010	2	4.78E-012	47	CONTIN
Menadione sodium bisulfite	7.48E-011	3	5.46E-012	38	CONTIN
N-Acetyl Cysteine	1.31E-010	2	8.82E-012	25	CONTIN
Sodium Lipoate	6.88E-011	3.4	2.34E-011	9.9	HDRC triexponential
	3.54E-011	6.5	-	-	CONTIN

Table 1 Hydrodynamic radius of the various modes present in solutions containing different modifiers along with HGD

CHAPTER 2: COLLAGEN TYPE II FIBROGENESIS

Collagen type II is an essential structural protein that organizes into long fibers[3]. This propensity to assemble into fibers has been attributed to the charge carrying amino acids on the surface of the protein[20]. Structurally, the protein is a rod-like right-handed helix formed by the association of three left-handed helices. Sveta et al. found that the ionic strength of solvent tunes the electrostatics between them proteins to form a fiber.[20] Increasing ionic strength screened the electrostatic attraction between them, leading to a lesser amount of collagen fibers with slower growth kinetics.

Apart from ionic strength influence of negatively charged polysaccharides like alginate [3], and hyaluronic acid[21]on Collagen type II growth kinetics have been performed. In the presence of Alginate, the fibers obtained were thicker, but the kinetics was slowed down. In comparison, the presence of hyaluronic acid altered the growth kinetics for Collagen type II only slightly in the study by Chang et. al.

Across the literature, Collagen fibrogenesis is studied experimentally by measuring the change in turbidity as a function of time[22], as seen in figure 16. The early time points of the measurement where there are no changes in turbidity comprise the lag phase, highlighted as the gray area in figure 1, and this time duration is the lag time. The rapid increase following the lag phase is the growth phase, highlighted in yellow in figure 16. While Silver et al. defines the growth rate as the inverse of the time difference between the end of the growth phase and the lag time, in this study, we define it as the slope of the tangent to the growth phase.

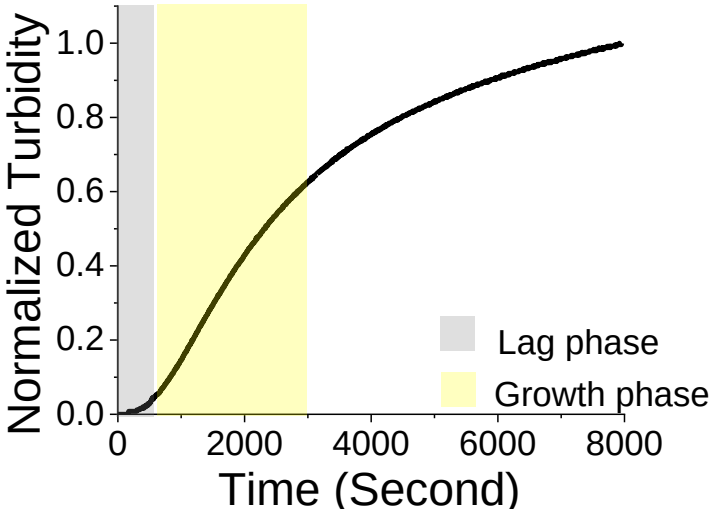

Figure 16 Representative data for Collagen type II fibrogenesis measurement using Turbidity, where the lag phase of the kinetics is highlighted in gray and the growth phase in yellow.

Additionally, previous studies by Silver et al. and Chang et al. employ pseudo-first-order kinetics to explain the kinetics. Instead, we employ classical nucleation theory, typically used in crystallization, to explain the Collagen fiber formation kinetics. The motivations for applying principles of crystallization to Collagen growth are because of the similarities between the phenomenon. These are an initial lag followed by growth, a critical concentration required for the assembly to take place, large changes in the lag time on small changes in concentration, and temperature dependence of lag time at a fixed concentration of Collagen.

According to classical nucleation theory for crystallization, the initial lag arises from the process of the formation of nuclei. This nucleation time (τ_{nuc}) is proportional to the exponent of the nucleation free energy barrier($\Delta\mu$) as in equation (1). Thus, lag time acts as a measurable estimate of the barrier height[23].

$$\tau_{\text{nuc}} \propto e^{\frac{\Delta\mu}{KT}} \quad \ldots (1)$$

This nucleation free energy barrier, in turn, is dependent on the concentration of the protein by the equation (2), where C is the concentration of the protein and Cm is the critical concentration required to initiate the process.

$$\tau_{\text{nuc}} \propto \frac{1}{\ln\left(\frac{C}{C_m}\right)} \quad \ldots (2)$$

Rearranging the above equation, we see that nucleation time and concentration of the protein are inversely related. This relationship shows us that only at concentrations beyond the critical concentration would the system possess enough energy to surmount the nucleation barrier.

$$\frac{1}{\tau_{\text{nuc}}} \propto \ln(C) - \ln(C_m) \ldots (3)$$

On the other hand, at a constant concentration above the critical concentration, the nucleation time (τ_{nuc}) and temperature (T) are inversely related by the following relation, where Tm is the disassembly or melting temperature.

$$\ln(\tau_{\text{nuc}}) \propto \frac{1}{(T_m - T) * T} \quad \ldots (4)$$

This relationship essentially shows that with the support of additional energy in the system in the form of heat, the nucleation barrier could be crossed quickly as long as $T < T_m$.

To explain the growth phase of Collagen fibrogenesis, we borrow from the secondary nucleation theory of polymeric systems. Here, the process of attachment of the polymer to the growth front has the nucleation barrier, resulting in the following relationship between growth rate and the growth rate, temperature (T), and the temperature of disassembly, T_m:

$$\ln(G) \propto \frac{1}{(T_m - T) * T} \quad \ldots (5)$$

In this chapter, we evaluate whether Collagen fibrogenesis kinetics follows the classical nucleation theory. Specifically, we evaluate whether the lag time is susceptible concentration and if lag time is susceptible to the temperature at a fixed concentration (at a fixed barrier for nucleation), all under physiological conditions of pH = 7.2.

Method

Instrumentation

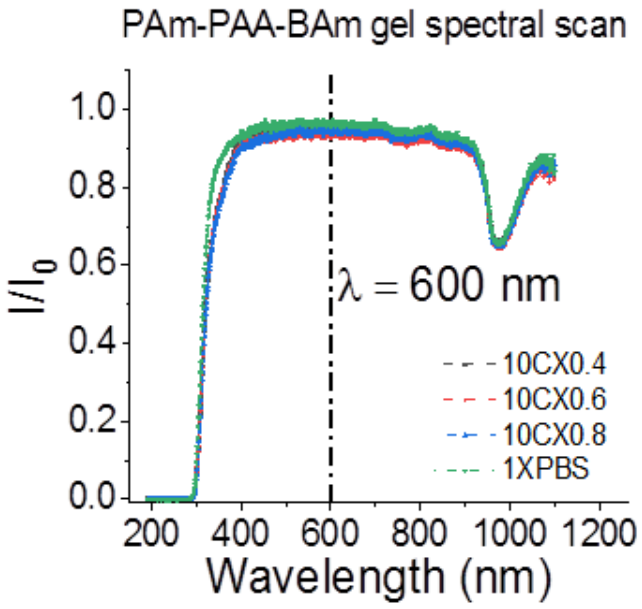

Figure 17 Absorption spectrum of the matrix gels (10% Charge density 0.4% crosslinking density – 10CX0.4, 10% Charge density 0.6% crosslinking density – 10CX0.6, 10% Charge density 0.8% crosslinking density – 10CX0.8, and buffer solution 1xPBS) into which the Collagen type II fibers are to be grown

In this study, turbidity is measured at a wavelength of 600 nm on a Shimadzu 3600 UV-Vis spectrophotometer. The sample was placed in a 6Q quartz cuvette while taking the measurement. The wavelength of 600 nm was chosen as both the protein (Collagen type II) and the gel matrix the Poly (Acrylamide-co-sodium acrylate), in which further experiments were planned, doesn't absorb light at this wavelength, as can be seen from figure 17.

Sample preparation

All experiments performed in this study are at a final pH = 7.2 in a Tris-HCl buffer with a final concentration of 150 mM, after collagen stock addition. Collagen stock solution was prepared by dissolving commercially obtained Bovine Collagen type II (purified from Bovine nasal septum) by Elastin products Inc. (product # CN276) in 12 mM HCl. This stock was stored on ice till the experiment began and is prepared on the day of the fibrogenesis experiment. Using old stock, for example, using a 3-day-old stock solution didn't result in a lag phase, as seen in figure 18.

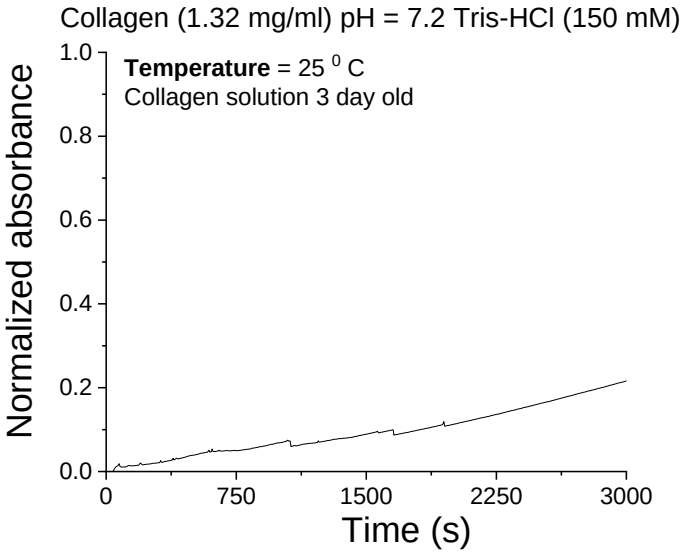

Figure 18 Turbidity measurement of Collagen type II 1.32 mg/mL in TrisHCl pH = 7.2 from a stock collagen solution stored for 3 days.

As the stock must be stored on ice until fiber formation is initiated, equilibrating to a temperature of interest was challenging. Directly adding the cold Collagen stock solution or incubating the solution for 15 min at room temperature closer gave rise to an upturn at early time points that can be attributed to the temperature relaxation of the sample, as seen in figure 19.

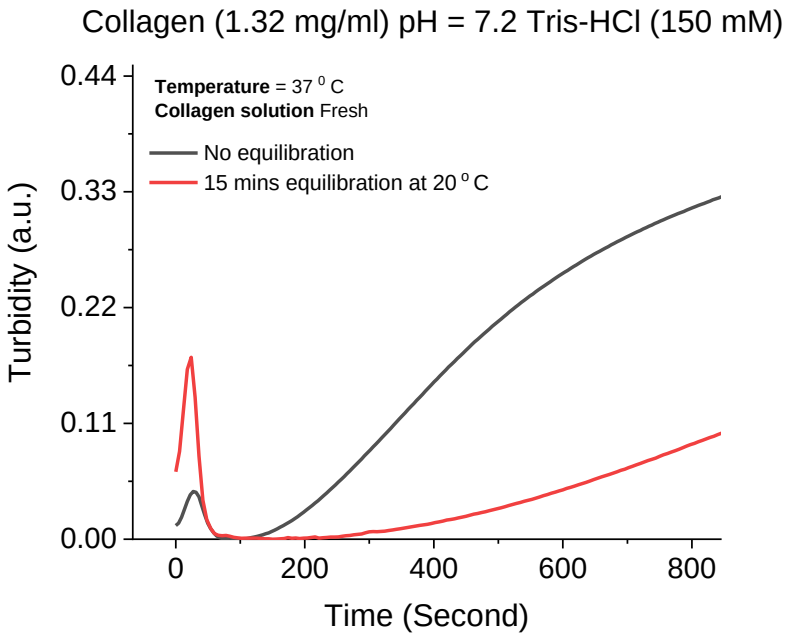

Figure 19 Turbidity measurement of Collagen type II (1.32 mg/mL) fiber growth in TrisHCl pH = 7.2 at 37 oC after no incubation (black) and 15 min equilibration at 20ºC displaying a peak at early time point.

To instantly place the collagen solution at a temperature of interest t_f, without equilibration, the buffer solution is heated to a higher temperature t_2, based on equation (1), and cold collagen stock solution at temperature t_1 is added to it. In this equation, m1 and m2 are the mass of the collagen stock volume to be added and the mass of the final solution,

respectively. The primary assumption in applying this equation is that parent stock solutions and the final mixture have the same Cp.

On addition of the cold collagen stock to the hot buffer, as measured in the lab, the temperature of interest is obtained. For example, to obtain an 800 µl Collagen type II solution at 37 ^{o}C from a 200 µl collagen stock stored at 4 ^{o}C, the 600 µl buffer must be heated to 48.1 ^{o}C. All of this takes place while the cuvette for the spectroscopic measurement is incubated at the final temperature of interest t_f for at least 10 minutes.

$$t_f = \frac{(m_1 t_1 + m_2 t_2)}{(m_1 + m_2)} \quad \text{....(6)}$$

Timing the experiment

The fiber formation begins as soon as the Collagen stock is added to the buffer. This phenomenon was noted when the solution turned visibly turbid while dialyzing Collagen dissolved in 12 mM HCl into Tris HCl buffer at 4 ^{o}C, seen in figure 20, indicating the formation of fibers

Figure 20 Collagen fibers formed on dialysis into Tris HCl

The experiment was timed via two timers, one manual timer that measured the amount of time it took to transfer the stock Collagen solution into the buffer, mix it and add the solution to the cuvette for making the measurement. The other timer is inbuilt in the

spectrophotometer; it was once that this timer had started; the manual timer was turned off.

Depending on the viscosity of the stock solution, mixing times varied. A graphic explaining the methodology of the experiment is presented in figure 21

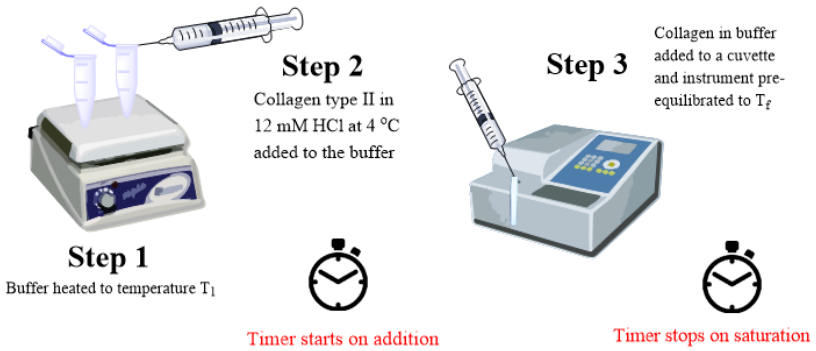

Figure 21 A graphic explaining the protocol of the

Data Analysis

Due to the instrumental constraints, the data is recorded in discrete intervals of 2.5s. This discretization makes analysis based on first or second derivate estimates unfruitful, as the changes are too small for the derivate methods, as seen from figure 22. Instead, the experimentally obtained normalized turbidity is averaged over 3 independent measures and fitted to a Logistic equation. The data generated in this study fitted to the logistic equation displayed in equation 7.

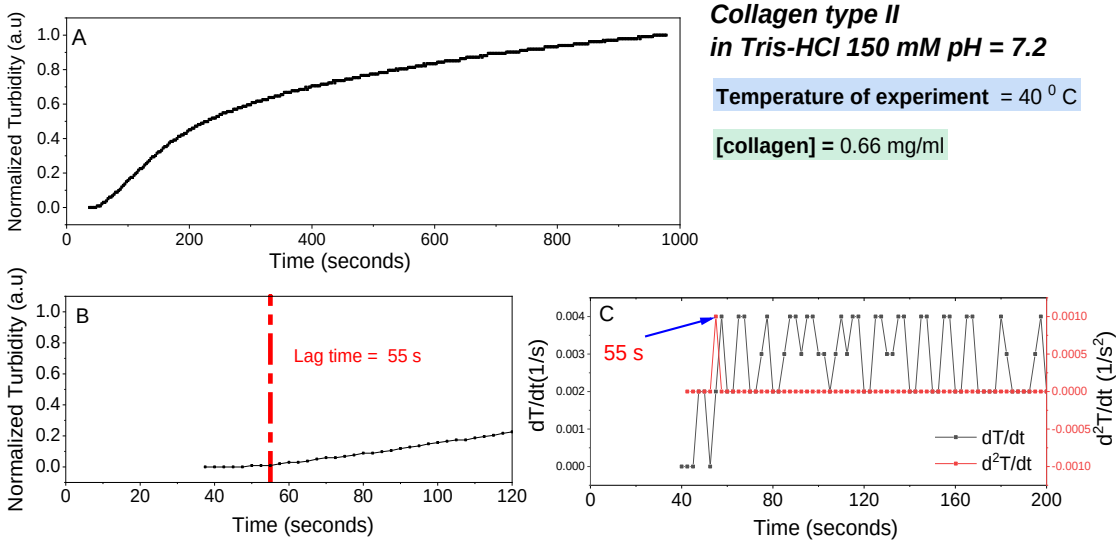

Figure 22 A. Normalized turbidity as a function of time for Collagen 0.66 mg/mL in Tris HCl at 40°C, B. Lag time estimation by visual inspection C. Lag time estimation by calculation of first and second derivate by Forward Difference method.

$$\text{Normalized turbidity} = 1 - (1/\ (1 + (x/x_0)^{p}) \quad \ldots\ldots (7)$$

The Levenberg–Marquardt algorithm in Origin is utilized for fitting the raw data to the equation (2); parameters x0 and p are varied to obtain a good fit. Once a logistic fit is obtained, at the point x1, the midpoint of the linear regime, a tangent is drawn. The x-intercept of this tangent gives us the lag time, and the slope gives the growth rate. In figure 23, the dataset corresponding to collagen concentration 0.165 mg/mL at 40 °C has been fit to a logistic curve, and the tangent has been drawn at x0. The tangent follows the equation y = 1.04E-3x -0.19578, resulting in a lag time of 188s for this data and a growth rate of 1.04E-3 (1/s).

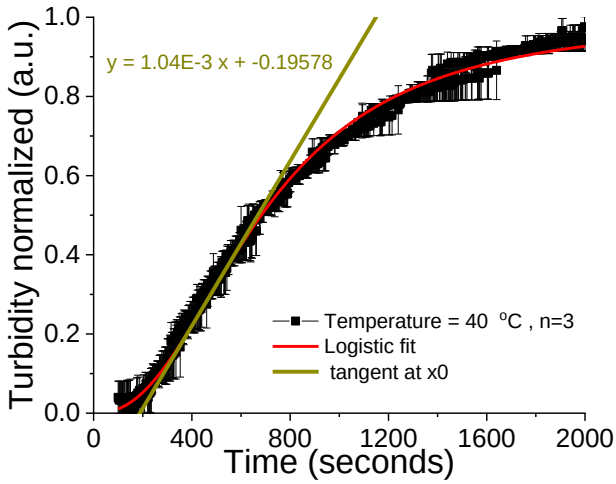

Figure 23 Data for collagen concentration 0.165 mg/mL at 40 °C in black, the logistic fit in red, and the tangent drawn in the linear segment to estimate a

Results and discussion

To evaluate whether Collagen fibrogenesis follows classical nucleation theory, we study the relationship between the lag time or nucleation time and growth rate with the experimental parameters of temperature and Collagen concentration. All the studies are performed in Tris- HCl pH=7.2 buffer. The constant concentrations studies were performed at a concentration of 0.165 mg/mL in the experimental temperatures of 31,34,37,40, and 43 ° C. The isothermal studies were performed at 40 ° C in the concentrations of 0.165, 0.33,0.5,0.66,1 and 1.325 mg/mL.

Concentration dependence of growth kinetics

At a constant temperature, increasing collagen concentration reduced the lag time for Collagen, as seen in figure 24. Additionally, under the experimental methods described in this chapter, a minimum concentration of 0.125 mg/mL is required to observe any Collagen fiber growth. These features are indicative of the nucleation growth phenomenon.

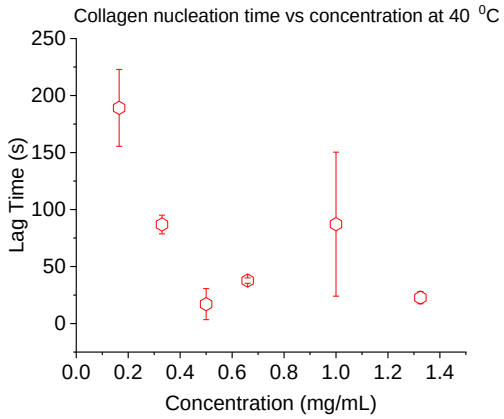

Figure 24 Collagen type II nucleation time decreases as a function of concentration at 40 ° C

On the other hand, the growth rate behaves non-monotonically with respect to concentration, as seen in figure 25.

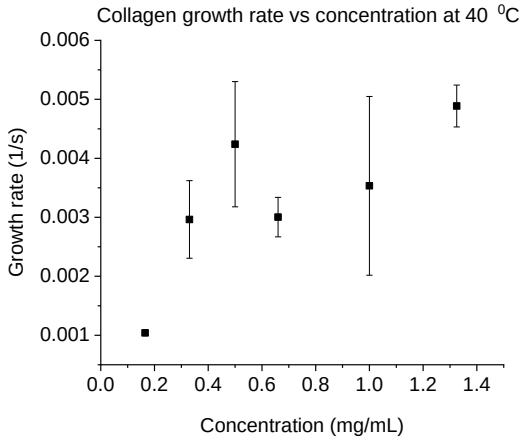

Figure 25 Collagen type II growth rate displaying non-monotonic dependency on concentration at 40 ° C

To further evaluate whether this decrease in lag time with an increase in concentration follows the functional form expected from nucleation growth kinetics, inverse lag time and ln C were plotted. On simplifying equation 3, we obtain the following relation (8), indicating that for a system with nucleation growth, ln(C) and inverse lag time are linearly related.

$$\ln(C) \sim \frac{1}{lag\ time} \ldots. (8)$$

Our experimental data does not fit a straight line (figure 26). This informs us that the lag phase does not follow nucleation- growth kinetics.

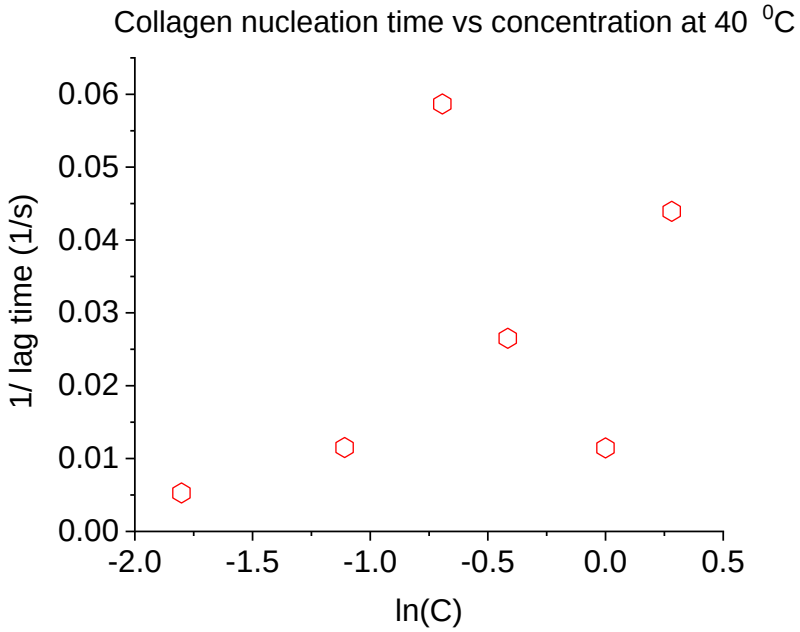

Figure 26 Inverse of lag time and lnC plot for collagen fibrogenesis at 40

Temperature dependence of growth kinetics

At a constant concentration of 0.165 mg/mL, with increasing temperature, the lag time for Collagen fibers reduced, as seen in figure 11. This dependence is expected as elevated temperatures reduce the energy barrier for fiber formation. To evaluate the specific functional relationship between Lag time and temperature, a semi-log plot between log nucleation time and temperature in figure 27.

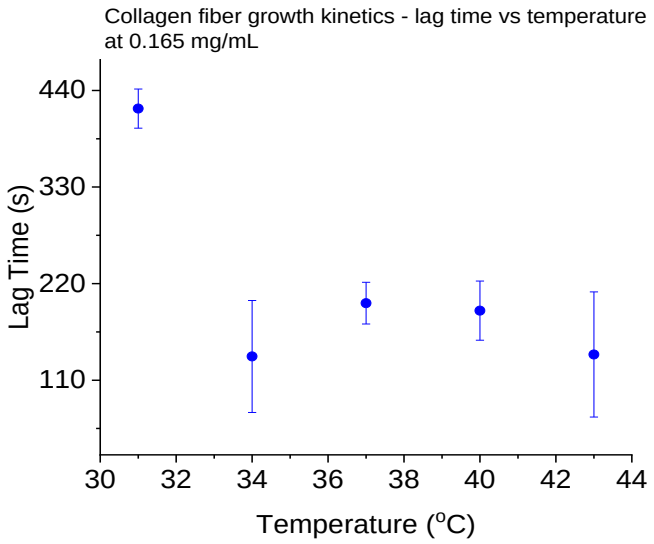

Figure 27 Collagen type II nucleation time decreases as a function of temperature at 0.165 mg/mL

For a nucleation growth phenomenon, the log of nucleation time is related to the temperature quadratically. We can obtain this relation by simplifying equation (4) further,

$$lag\ time \sim \frac{1}{Tm*T-T^2} \ldots (9)$$

Our experimental data did not fit this functional form, as seen in figure 28, concurring with the outcomes from the previous section that the early lag phase in Collagen fibrogenesis does not obey nucleation-growth kinetics. Contrastingly, the growth rate behaves non-monotonically with respect to temperature (figure 28). Under the experimental conditions

described in this chapter, at the philological temperature of 37 ^{o}C fastest growth rate for collagen fibers was observed at 0.165 mg/mL.

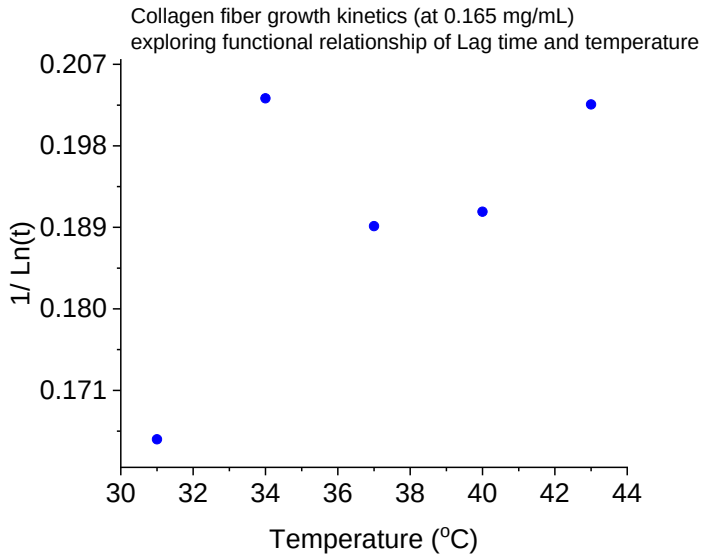

Figure 28 Inverse ln(lag time) vs Temperature for Collagen concentration 0.165

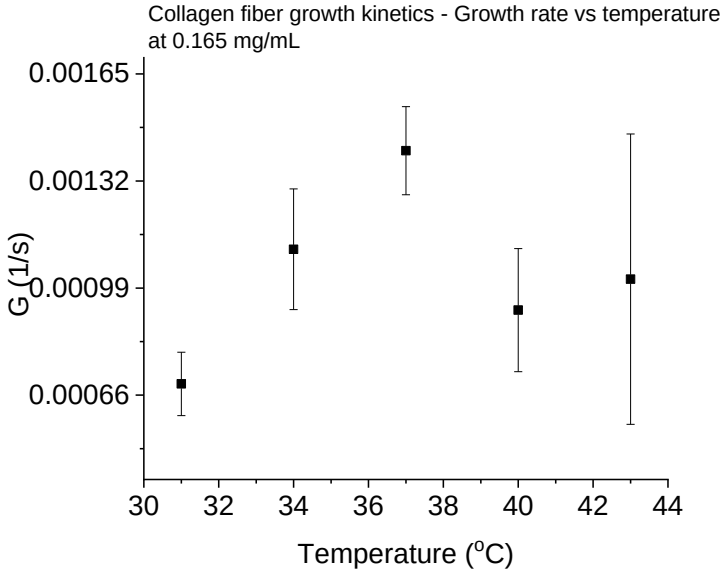

Figure 29 Collagen type II growth rate as a function of temperature at 0.165 mg/mL

To verify if the growth phase of the collagen fibrogenesis kinetics followed the secondary nucleation phenomenon, inverse ln growth rate and temperature were plotted, as seen in figure 29. On simplifying equation (5), it is known that for secondary nucleation, lnG must be quadratic in temperature.

$$\frac{1}{\ln(G)} \propto (T_m * T - T^2) \ldots. (10)$$

But in our experimental values we observed a linear relationship (Figure 30).

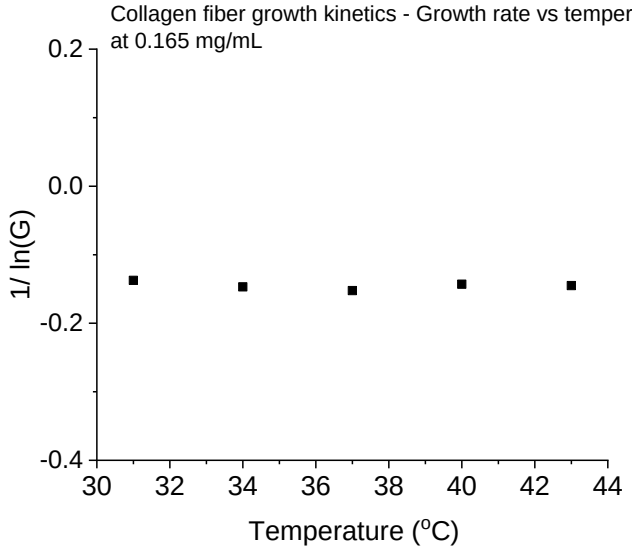

Figure 30 Inverse ln(Growth rate) vs Temperature for Collagen concentration 0.165 mg/mL

Conclusions

Collagen fibrogenesis, performed according to the methods described in this chapter, displayed the presence of a critical concentration for fibrogenesis. And, while the lag time at a constant temperature decreased with increasing protein concentration, it did not follow the functional form of nucleation growth as hypothesized in the beginning. The growth rate at various temperatures at a fixed concentration also did not follow the functional relationship observed in secondary nucleation. The limitations of the

experimental method confine the investigation to a relatively narrow parameter space. Under these conditions, our results do not confirm the initial hypothesis.

APPENDIX 1: FACTORS INFLUENCING LIGHT SCATTERING IN POLY ACRYL AMIDE ACRYLATE GELS

Introduction

The work in this appendix was initiated with the objective of making composites of Collagen fibers and Polyacrylamide acrylate gels. Over the course of this study the goal was to optimize parameters of the gel like crosslinking density, charge density of the monomer, and the ionic strength of the swelling solvent to obtain intensity correlation functions that were suitable for further analysis. For the sake of discussion, the initial amplitude of the intensity correlation function $g_2(q,\tau)_{\tau \to 0}$ is referred to as β. This β is different from the β as seen from equation 1, which is a geometric factor relating to the coherence volume for ergodic systems[5].

The arbitrary thumb rule of the lab of obtaining correlation functions with an amplitude β > 0.4 was utilized as a cutoff for a function suitable for further analysis. The rationale behind this arises from the fact that a small amplitude of the intensity correlation function shows that the intensity fluctuations are reduced, either owning a small concentration of scatterers or non-decaying concentration fluctuation.[24]

Methods

Synthesis of Poly (acrylamide-co-sodium acrylate) gel

The gels used in this study were prepared by free radical polymerization catalyzed by Tetramethyl ethylenediamine (TEMED) and Ammonium per sulfate (APS). The Poly (acrylamide-co-sodium acrylate) gels in the rest of this study follow the following nomenclature pattern based on the mole% of the charged monomer (p%) and crosslinker(q%): pCXq. For example, for a 10% charge density and 0.2 % crosslinking density the gel would be named as 10CX0.2

The method of synthesis as described in the thesis by Rahalkar et.al was followed[24]. Suitable amounts of monomer and crosslinker solutions based on the % change and crosslinking density were added, keeping the total concentration (monomers+ crosslinker) fixed to 5.25E-01 M. Sodium acrylate monomer solution of 20% (w/w) was prepared in the lab, while commercially prepared Sodium acrylate solution of 40% (w/v) and commercially prepared Bis Acrylamide solution of 2 % (w/v) was used for the synthesis. Following the addition of the monomers and crosslinkers, swelling solvent was added to bring the entire solution up to the volume of interest. This pre-gelation solution was flushed with nitrogen briefly, following which 19 moles % of TEMED per mole of monomers+ crosslinker and 0.4 mole% of APS per mole of monomers+ crosslinker were added to initiate the gelation. APS solution of 0.1 g/mL was prepared fresh each time the gels were synthesized.

As an example, the following table contains the specific amounts of the chemicals used to prepare a 10CX0.2 (10% charge density and 0.2 % crosslinking density) sample in a 10 mL volume vial.

After initiating gelation, the solution was quickly filtered using a 0. 22 μm PVDF filter into glass vials for light scattering. The light scattering vials were sealed on the top with parafilm and filtered nitrogen was supplied to the vial via a home-step up. The home setup comprised of a nitrogen line with a syringe at the end whose nozzle was connected to a 0. 22 μm PVDF filter. The filtered nitrogen was delivered into the light scattering vial via a 22G needle. The sample was left undisturbed until gelation was complete, which approximately for low crosslinking densities took an hour.

Name of the compound	Concentration (g/mL)	Amount (in g)	# moles	Moles: total moles of monomer and crosslinker	Volume added (mL)	mole%
Acryl amide	4.0E-01	3.4E-01	4.8E-03	9.1E-01	8.5E-01	90.9
Sodium Acrylate	2.0E-01	4.4E-02	4.7E-04	8.9E-02	2.2E-01	20.0
Bis acrylamide	2.0E-02	1.6E-03	1.0E-05	2.0E-03	8.1E-02	2.7
TEMED		1.2E-02	1.0E-04	1.9E-02	1.5E-02	1.9
APS	1.0E-01	5.0E-03	2.2E-05	4.2E-03	5.0E-02	0.4

Table 2 Above table contains the specific amounts of the chemicals used to prepare a 10CX0.2 (10% charge density and 0.2 % crosslinking density) sample in a 10 mL volume vial

Swelling the gel for light scattering

To check if gelation was complete the vial was inverted, if the gel had formed it would remain stuck to the bottom of the tube, otherwise the solution was left a little longer to form a gel. Once gelation was complete the gel front was marked with a sharpie, and the suitable swelling solution was added to it. The change in the height of the gel front was monitored over a period, and every day the swelling solvent was changed. The changing of the swelling solvent comprised of taking out the remaining solvent and adding fresh filtered solvent over the gel front. Once the gel's growth front had stopped moving the gel was said to have reached swelling equilibrium. In this chapter all the samples were swollen in 1X PBS, except for the

study where salt concentration of the swelling solvent is varied by varying the NaCl concentration.

Method of Light scattering

The light scattering experiment was performed on light scattering setup with an ALV goniometer which has an ALV-5000/E correlator, a 2 W Argon source of 514.5 nm was used as a light source. The incident intensity of the light source was kept constant across the study over the various samples at approximately 207500 a.u., a value arbitrarily chosen as it was the incident intensity on the first sample in the study. Correlation functions for the gels were measured across 3 arbitrarily chosen physical locations or orientations in the tube containing the gel at an angle $\theta = 30$ degrees for a duration of 100 seconds.

Results and discussion

In this chapter, we evaluate which of our experimental parameters of interest (solvent salt concentration, crosslinking density and charge density on the polymer backbone) control the value of the $t = 0$ asymptotic intercept of the intensity correlation function, β. In case of ergodic systems this is a purely instrument-dependent constant, but for non-ergodic systems, the scattering from static inhomogeneous influences this value.

i. Variation in β as a function of crosslinking density of the crosslinker

Better quality correlation functions as characterized by $\beta > 0.4$ were observed for gels with a lower crosslinking density (10CX0.2 and10CX0.6) in figure 31 (a) and (b). These gels with low crosslinking (10CX0.2) density also displayed less variation in the correlation function, as the correlation function measured across the three orientations completely overlap across all relaxation times. The decreasing β for the highly cross-linked systems could be explained by the increased static scattering from these crosslinking points.

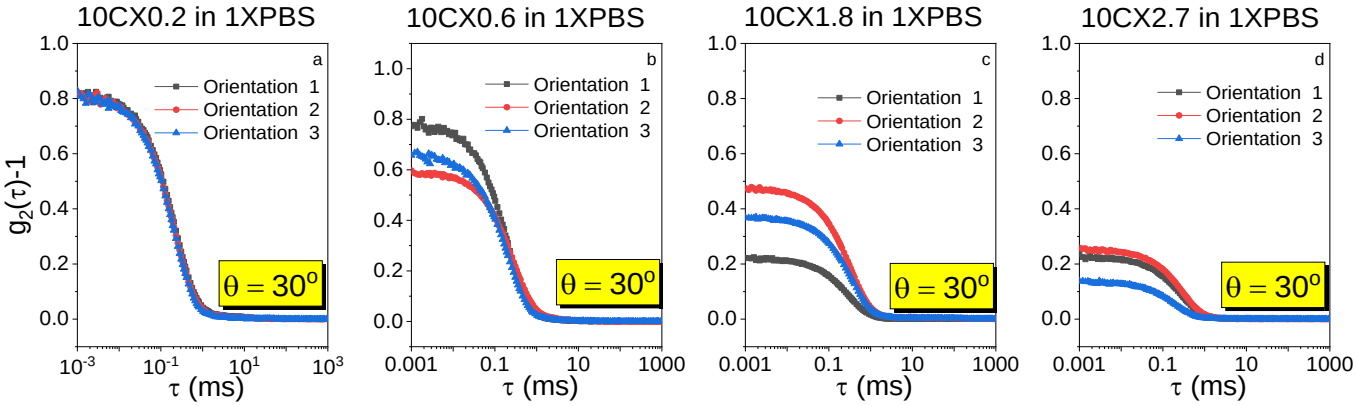

Figure 31. correlation function at θ = 30 degrees across 3 arbitrary orientations for a. 10CX0.2 swollen in 1xPBS b. 10CX0.6 swollen in 1xPBS c. 10CX0.8 swollen in 1xPBS d. 10CX2.7 swollen in 1xPBS

ii. Variation in β as a function of charge density

The lower cross-linking density gels provided better correlation functions across low and high charge densities, as seen from figure 32 (a) and 2 (b), and these correlation functions overlapped across all relaxation times, indicating greater homogeneity in the gels. Contrastingly, the increase in crosslinking density by 10-fold dropped the β value on an average to below 0.4. Additionally, the correlation functions for these samples varied across orientations, indicating a large heterogeneity in these gels, as seen from figure 32 (c) and (d). Increasing the charge density on the backbone of the gel, did not improve the scattering of the highly cross-linked systems, indicating that the static scattering from the cross-linking points dominates the correlation function's quality.

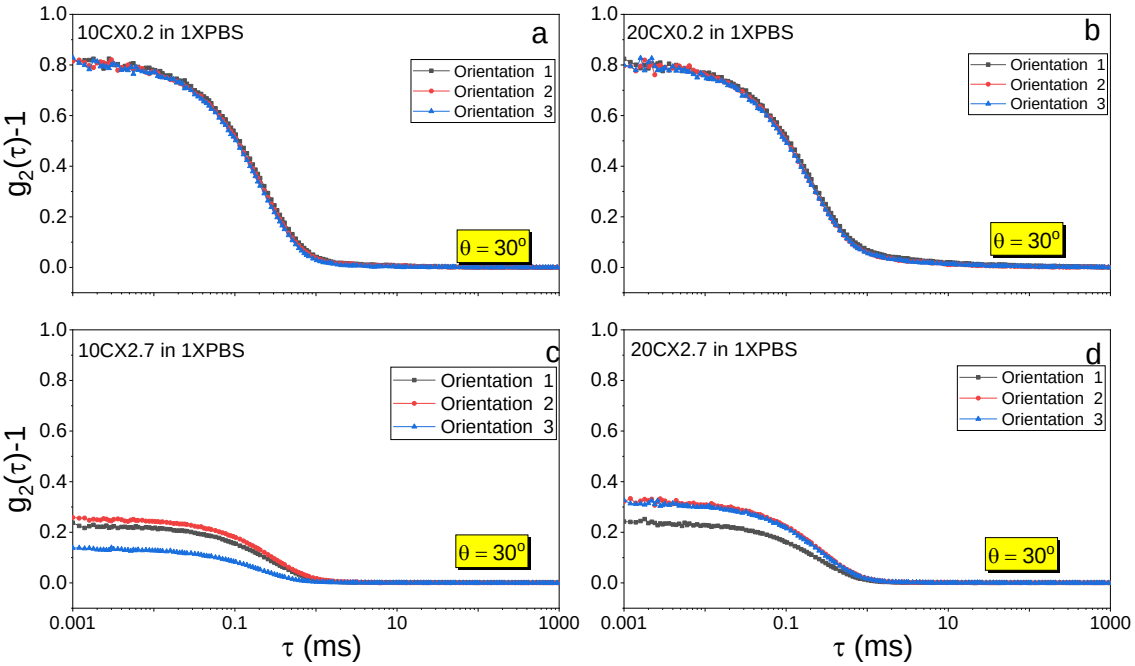

Figure 32 a. Correlation function at θ = 30 degrees across 3 arbitrary orientations for a. 10CX0.2 swollen in 1xPBS b. 20CX0.2 swollen in 1xPBS c. 10CX2.7 swollen in 1xPBS d. 20CX2.7 swollen in 1xPBS

iii. Variation in β as function of salt concentration of the swelling solution

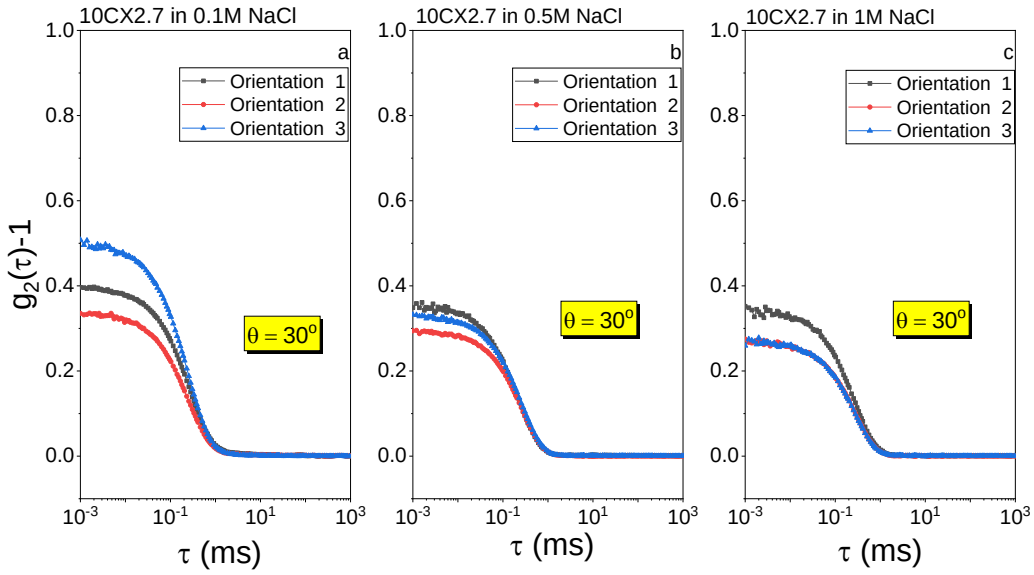

Figure 33 a. Correlation function at θ = 30 degrees across 3 arbitrary orientations for 10CX2.7 gel swollen in a. 0.1 M NaCl b. 0.5 M NaCl and c. 1 M NaCl

To evaluate if improving the contrast in scattering could improve the quality of scattering from highly cross-linked gels, we measured the correlation function for the 10CX2.7 gel with 0.1 M, 0.5 M and 1M salt concentration. The high contribution from the static scattering from these gels brought the β value on an average to below 0.4 irrespective of the salt concentration as seen from figure 33 (a), (b) and (c) on the next page. Additionally, the lack of overlap between the correlation functions at slower relaxation times indicate that these gels are highly heterogenous.

Conclusions

In this study for the first time we report an evaluation of the heterogeneity in high cross-linking density Poly (acrylamide-co-sodium acrylate) gels. We found that gels with low cross-linking densities (of 0.2 to 0.8 mole %) displayed correlation functions that were significant with a $\beta > 0.4$. The correlation functions for the highly cross-linked gels displayed a consistently low β value.

Pusey et. al. has encountered a similar variation of β in Polyacrylamide gels and have attributed these to frozen-in fluctuations or inhomogeneities. Additionally, they also observed that for a fixed polymer concentration with increasing crosslinking density the amplitude of $g_2(q,\tau)$ decreased[25]. Despite increasing the ions on the backbone, with an increased charge density or increasing the salt concentration to improve the contrast, the static scattering from the cross links dominated bringing down the β value.

Additionally, for future studies of Collagen-gel composites with Poly (acrylamide-co-sodium acrylate) gels, lower cross-linking densities are better suited as the correlation functions can be analyzed for evaluating the effect of embedding Collagen on the polymer chain dynamics.

REFERENCES

1. Cox, M. *et al. Lehninger Principles of Biochemistry*. (United Kingdom: W. H. Freeman, 2005).

2. Moreau, K. L. & King, J. Hydrophobic core mutations associated with cataract development in mice destabilize human ??D-crystallin. *J. Biol. Chem.* **284**, 33285–33295 (2009).

3. Kuo, S. M., Wang, Y. J., Weng, C. L., Lu, H. E. & Chang, S. J. Influence of alginate on type II collagen fibrillogenesis. *J. Mater. Sci. Med.* **16**, 525–531 (2005).

4. Hiemenz, P. C. & Lodge, T. P. *Polymer Chemistry - Paul C. Hiemenz, Timothy P. Lodge - Google Books*. (CRC Press, 2007).

5. Berne, B. J. & Pecora, R. *Dynamic Light Scattering - Google Books*. (Dover Publications, 2013).

6. Acosta-Sampson, L. & King, J. Partially Folded Aggregation Intermediates of Human ??D-, ??C-, and ??S-Crystallin Are Recognized and Bound by Human ??B-Crystallin Chaperone. *J. Mol. Biol.* **401**, 134–152 (2010).

7. Evans, P. *et al.* The P23T cataract mutation causes loss of solubility of folded γD-crystallin. *J. Mol. Biol.* **343**, 435–444 (2004).

8. Vendra, V. P. R. & Balasubramanian, D. Structural and aggregation behavior of the human γD-crystallin mutant E107A, associated with congenital nuclear cataract. *Mol. Vis.* **16**, 2822–8 (2010).

9. Serebryany, E. *et al.* Aggregation of Trp > Glu point mutants of human gamma-D crystallin provides a model for hereditary or UV-induced cataract. *Protein Sci.* **25**, 1115–1128 (2016).

10. Sharma, K. K., Kumar, R. S., Kumar, G. S. & Quinn, P. T. Synthesis and characterization of a peptide identified as a functional element in ??A-crystallin. *J. Biol. Chem.* **275**, 3767–3771 (2000).

11. Nagaraj, R. H. *et al.* Therapeutic potential of α-crystallin. *Biochimica et Biophysica Acta - General Subjects* **1860**, 252–257 (2016).

12. Georg, B. & Mohr, R. Macromolecular Assemblies : Human Gamma- Crystallin Protein , Glutamic Acid Bottle Brushes , And Hyaluronic Acid Gels. (2013).

13. Mohr, B. G. R. Macromolecular assemblies: Human γ-crystallin protein, glutamic acid bottle brushes, and hyaluronic acid gels. *Doctoral Dissertations Available from*

Proquest (2013).

14. Broide, M. L., Berland, C. R., Pande, J., Ogun, O. O. & Benedek, G. B. Binary-liquid phase separation of lens protein solutions. *Proc. Natl. Acad. Sci. U. S. A.* **88**, 5660–4 (1991).

15. Pande, J. *et al.* Suppression of phase separation in solutions of bovine gamma IV-crystallin by polar modification of the sulfur-containing amino acids. *Proc. Natl. Acad. Sci. U. S. A.* **88**, 4916–20 (1991).

16. Clark, J. I. & Benedek, G. B. The effects of glycols, aldehydes, and acrylamide on phase separation and opacification in the calf lens. *Investig. Ophthalmol. Vis. Sci.* **19**, 771–776 (1980).

17. Pande, Jayanti; Ogun,Olutayo; Nath, Cheryl; Benedek, G. Suppression of Phase Separation in Bovine γIV Crystallin Solutions: Effect of Modification by Charged Versus Uncharged Polar Groups. *Exp. Eye Res.* **57**, 257–264 (1993).

18. Ron, A. J. B. *et al.* Nutrition supplements and the eye. *Eye (Lond).* **12 (Pt 1)**, 127–133 (1998).

19. Mohr, B. G., Dobson, C. M., Garman, S. C. & Muthukumar, M. Electrostatic origin of in vitro aggregation of human ??-crystallin. *J. Chem. Phys.* **139**, 1–13 (2013).

20. Morozova, S. & Muthukumar, M. Electrostatic effects in collagen fibril formation. *J. Chem. Phys.* **149**, 163333 (2018).

21. Kuo, S. M., Wang, Y. J., Niu, G. C. C., Lu, H. E. & Chang, S. J. Influences of hyaluronan on type II collagen fibrillogenesis in vitro. *J. Mater. Sci. Mater. Med.* **19**, 1235–1241 (2008).

22. Silver, F. H. & Birk, D. E. Kinetic Analysis of Collagen Fibrillogenesis: I. Use of Turbidity-Time Data. *Coll. Relat. Res.* **3**, 393–405 (1983).

23. MUTHUKUMAR, M. NUCLEATION IN POLYMER CRYSTALLIZATION. in *Advances in Chemical Physics* (ed. Stuart A. Rice) **128**, 1–63 (John Wiley & Sons, Inc., 2003).

24. Hulst, H. C. van de. *Light Scattering by Small Particles - Google Books*. (Dover Publications, 2012).

25. Joosten, J. G. H., McCarthy, J. L. & Pusey, P. N. Dynamic and static light scattering by aqueous polyacrylamide gels. *Macromolecules* **24**, 6690–6699 (1991).